Role of Erythrocyte Deformability During Capillary Wetting

Ronghui Zhou, Jason Gordon, Andre F. Palmer, Hsueh-Chia Chang

Department of Chemical and Biomolecular Engineering, University of Notre Dame, Notre Dame, Illinois 46556; telephone: 574-631-5697; fax: 574-631-8366; e-mail: hchang@nd.edu

Received 2 June 2005; accepted 19 July 2005

Published online 21 November 2005 in Wiley InterScience (www.interscience.wiley.com). DOI: 10.1002/bit.20672

Abstract: Deformability of erythrocyte was found to fundamentally alter the wetting dynamics of red blood cell (RBC) suspensions during their invasion into capillaries. Normal RBC suspensions failed to penetrate more than 1 cm into a glass capillary when the capillary radius was smaller than a critical value that is dependent on the erythrocyte concentration (about 50 μm for whole blood). In contrast, suspensions of rigidified RBCs, after cross-linking with different concentrations of glutaraldehyde or incubating with 100 ng/mL of an endotoxin, could penetrate any capillary larger than the erythrocyte dimension. The effect of RBC deformability on penetration was attributed to the enhanced shear-induced migration of normal deformable RBCs toward the capillary centreline, which imparted a higher average velocity to the RBCs than the average plasma velocity. As a result, the erythrocytes advanced into the capillary faster than the wetting meniscus, packing behind it to form a concentrated slug. This tightly packed slug had a high hydrodynamic resistance that could arrest the penetrating flow of concentrated suspensions into the small capillaries.

Keywords: membrane rigidity; wetting; shear-induced migration; suspension rheology

INTRODUCTION

The flow properties of blood suspensions are influenced by both red blood cell (RBC) deformation and aggregation. During sepsis, the appearance of pathological and rigidified forms of circulatory erythrocytes is postulated to produce abnormal cell–endothelial interaction, block capillary flow, and inhibit capillary exchange at important areas. All of these anomalous micro-circulation phenomena caused by rigidified erythrocytes can result in acute organ dysfunction (Baskurt et al., 1998; Hinshaw, 1996). Similar to septic RBCs, human blood substitutes from glutaraldehyde cross-linking of bovine RBCs can become rigid (Bellelli et al., 1988). These erythrocytes display increased mechanical and chemical resistance, but still bind oxygen reversibly. The optimal degree of glutaraldehyde cross-link to render the cells active but without altering the suspension hydrodynamics is thus of considerable interest.

Correspondence to: Hsueh-Chia Chang

Distinct rheological behaviors of deformable and rigid particle suspensions have been documented extensively for continuous shear flow in various channels (Brooks et al., 1970; Pries et al., 1992). Rigid RBC suspensions exhibit higher viscosity than normal blood suspensions, and this viscosity shows some shear-thinning effects at high shear rates and high RBC concentrations (Brooks et al., 1970). This shear-thinning viscoelastic rheology is thought to have an origin in RBC segregation. Unlike rigid RBCs, which segregate only at high concentrations, a single deformable RBC in a simple shear flow will drift away from a bounding wall (Olla, 1999). Hence, these segregation tendencies and the rheological anomalies are even more likely for healthy and deformable RBC suspensions. Due to this enhanced migration of deformable RBCs even at low concentration, the low-hematocrit RBC distribution in continuous flow through a capillary shows a clear marginal layer free of RBCs near the wall (Zhou and Chang, 2005). The thickness of the marginal layer increases with shear rate. As the plasma has a much lower viscosity than the homogeneous blood suspension, the effective suspension viscosity hence decreases with increasing shear due to this plasma-skimming phenomenon. This particular segregation and shear-thinning phenomenon for healthy blood suspensions, which is much more pronounced than those of rigid particles or rigidified RBCs, is commonly known as the Fahraeus–Lindqvist effect (Fahraeus and Lindqvist, 1931). The rheological effects of this phenomenon have been measured extensively since the earlier work of Haynes and Burton (1959).

We have recently uncovered yet another anomalous hydrodynamic phenomenon involving RBC suspensions (Zhou and Chang, 2005). Instead of continuous blood flow, we examined wetting blood flow into an open capillary where a meniscus advances ahead of the flowing suspension. We observe that whole blood fails to penetrate far into a glass capillary or a micro-needle with a diameter smaller than 100 μm, while such loading failure does not exist for plasma or RBC suspensions with lower hematocrit. This loading threshold is becoming a major technical obstacle in the diagnostic industry as miniature blood diagnostic kits become smaller. The penetration failure seems to be in contradiction

with the shear-thinning effect of Fahraeus–Lindqvist phenomenon at the high shear rate of 100/s when penetration fails. The marginal layer of the Fahraeus–Lyndqvist effect is responsible for the shear-thinning effect and should actually render the same suspension less viscous and hence easier to penetrate. There is hence a completely different hydrodynamic phenomenon at play during wetting. However, like the shear-thinning effect in continuous flow, we shall demonstrate that RBC segregation and aggregation play important roles in such wetting flow anomalies.

Numerous migration mechanisms have been suggested to explain particle aggregation at the capillary centreline in the Fahraeus–Lindqvist phenomenon, yet all are still under intense scrutiny. Migration of a single particle from a wall in a simple shear flow can arise due to asymmetry (Olla, 1999), deformability (Goldsmith and Mason, 1962; Olla, 1999), or inertia (Saffman, 1965). Typically, these suggested mechanisms break the fore-aft symmetry of the flow field around the particle to produce a privileged orientation that couples with a net hydrodynamic drag force in the cross-streamline direction to produce drift away from the wall. The asymmetric velocity perturbation produced by a non-spherical particle in the presence of a wall can hence contribute to this drift (Olla, 1999). Although a RBC is non-spherical, it still possesses a highly symmetric geometry about an axis. A RBC in capillary flow often orients its axis of symmetry with the capillary axis such that the fore-aft symmetry is again preserved (Minerick et al., 2002). For particles with fore-aft symmetry, external flow can only produce a zero-mean rotation of the particle, and hence no net transverse hydrodynamic force or drift can occur. Inclusion of inertia is also sufficient to break the symmetry of the velocity field around the particle. The extra inertial drag and compressive force due to the wall lead to a transverse migration with velocity $81\langle u\rangle a\gamma^{1/2}/6\pi v^{1/2}$ (Saffman, 1965), where $\langle u\rangle$ is the characteristic velocity, a is the particle radius, γ is the local shear rate, and v the kinematic viscosity. If the particle is spherical and rigid, only the inertial mechanism can produce a single-particle cross-streamline drift away from a flat wall. However, rigid particles $\sim$10 μm in radius equilibrate with the fluid velocity within a negligible inertial time of $\sim 10^{-5}$ s, and inertial effects are typically discounted in micro-capillary blood flow. For compressible particles, it is the small deformation produced by the strain of external flow that breaks the fore-aft symmetry. The compressive and tensile forces normal to the cell surface then result in a net transverse force and migration (Goldsmith and Mason, 1962). Hence, for a single RBC, deformation-induced migration is the most likely mechanism for radial segregation in a capillary. Because this migration mechanism involves a single particle without any stochastic component, the migration is ballistic and the mathematical description of the resulting cross-streamline particle flux resembles convective flux—a migration velocity can be obtained and will be presented subsequently.

Another distinct cross-streamline migration mechanism away from the wall is the shear-induced migration, which also involves a convection-like flux of rigid particles away from the wall. This mechanism results due to particle–particle interaction in a unidirectional shear flow. It necessarily involves multiple particles and is hence most pronounced at high particle concentrations. The particles are driven from a high shear-rate streamline at the wall to a low shear-rate streamline near the capillary axis in this shear-induced migration mechanism (Leighton and Acrivos, 1987). This drift is due to the higher interaction rate with other particles on the high-shear side of a reference particle because there is a larger difference in translational velocity between this particle and particles on nearby streamlines on that side. The higher frequency of interaction on the high shear side then propels the particle towards the low shear direction. As a result, a transverse gradient of the tangential shear-rate, (i.e., a transverse curvature in the tangential velocity) must be appreciable for this phenomenon to occur. The ''collision'' frequency measuring the frequency of particle interaction is roughly the shear rate $\gamma = \langle u\rangle/R$, where $\langle u\rangle$ is the characteristic velocity and R the characteristic transverse dimension of the channel, multiplied by the local particle volume fraction ϕ. However, a net migration can only result if a shear rate gradient $(\mathrm{d}\gamma/\mathrm{d}n)$ exists across the particle dimension a, and $\Delta\gamma = (\mathrm{d}\gamma/\mathrm{d}n)a$ is the appropriate shear rate to use for the interaction frequency $\Delta\gamma\phi$. Also, each interaction event should propel the reference particle by a length scale the same order as the particle size a. Hence, the migration velocity should scale as $(\mathrm{d}\gamma/\mathrm{d}n)\phi\mathrm{a}^2$. A characteristic shear rate gradient is $(\mathrm{d}\gamma/\mathrm{d}n) \sim \gamma/R \sim \langle \mathrm{u}\rangle/R^2$, and thus, the migration velocity scales as $\langle u\rangle\phi(a/R)^2$. Therefore, the characteristic migration time across the channel is $R/[\langle \mathrm{u}\rangle\phi(a/R)^2]$ and the induction distance for this segregation to develop in the flow direction is $L_\mathrm{t} = (R^3/a^2)/\phi$. This induction length will be shown to play an important role in the segregation dynamics of deformable RBCs responsible for loading failure. The sensitive dependence on the particle concentration ϕ and the particle size a, due to the multi-particle interaction origin of shear-induced migration, is evident in the induction length.

There are other transport mechanisms across streamlines due to particle-particle interactions, but they are driven by transverse concentration gradients and the resulting viscosity gradients. These two mechanisms are diffusive in nature as they tend to homogenize any concentration gradient, and they have a diffusivity that scales as $\gamma\phi\mathrm{a}^2$ (Phillips et al., 1992). As a result, the diffusion time for both mechanisms and the associated induction length are identical to that of shear-induced migration. In particular, the induction length is also $L_\mathrm{t} = (R^3/a^2)/\phi$ in a suspension of concentrated rigid particles. Hence, it requires the same channel length to segregate and homogenize by these multi-particle mechanisms, and which one occurs depends on the local flow field and shear-rate gradient.

The present study is designed to study the relationship between the various migration mechanisms, particularly the single-particle migration mechanism due to deformation and the multi-particle shear-induced migration and diffusion

mechanisms, on the wetting dynamics of blood being loaded into a micro-capillary. All mechanisms will be demonstrated to occur at some stage during the penetration failure. However, the key driving mechanism will be shown to be the single-particle deformation-induced migration mechanism. As a consequence, RBCs possessing different degrees of rigidity, as a result of treatment with either glutaraldehyde or lipopolysacchride (an endotoxin used to induce sepsis), do not suffer penetration failure. Our study suggests the potential use of wetting failure as a straightforward indicator of cell deformability.

MATERIALS AND METHODS

Citrated fresh normal bovine red blood cells (Animal Technologies Inc., Tyler, TX) upon receiving were re-suspended in standard 0.9% saline solution (Phoenix Scientific, Inc., St. Joseph, MO) to prepare RBC suspensions of different hematocrit concentrations $\phi_0 = 1$, 5, 10, 20, 30, 40, and 60% maintained at a pH of 7.4. The initial erythrocyte volume fraction was determined to be roughly 95 to 100% by measuring the hemoglobin (Hb) concentration via a modified cyanomethemoglobin method (Oser, 1965). Micro particles based on polystyrene (5 μm, Fluka Chemie) at concentrations of 1 and 5%, suspended in saline solution were also prepared for contrast as known rigid particles. The addition of small amount of plasma or RBC re-suspended in PBS has negligible effects on the measurement.

Lipopolysaccharide from *E. coli* O111:B4 (an endotoxin) was purchased from Fisher Scientific, and dissolved respectively into RBC suspensions at 37°C to prepare endotoxin treated red blood cell suspensions using different endotoxin concentrations at 20, 100, and 1 mg/mL. Experiments were carried out 30 min after mixing the endotoxin with the RBC suspensions.

For the cross-linking reaction, glutaraldehyde (25%) was obtained from Sigma. Prior to reaction, RBCs were washed with sterile (via 0.2 μm filtration), cold phosphate buffered saline (PBS, pH = 7.4) in order to remove free Hb and remaining plasma proteins. The RBCs were then resuspended in PBS to give a Hb concentration of 3.5 mM. The cross-linking reaction was carried out at 2 different molar ratios of Hb (within the RBCs) to glutaraldehyde (1:1 and 2:1) for 12 h. RBCs (12 mL, 3.5 mM Hb) and glutaraldehyde were each transferred to a single 50-mL centrifuge tube wrapped in aluminium foil (glutaraldehyde is light sensitive), and the tube was placed onto a 3-D rotator within a 4°C refrigerator for subsequent reaction. To quench the cross-linking reaction, sodium borohydride ($NaBH_4$) was added at a 2:1 molar ratio to the initial glutaraldehyde concentration. The quenching reaction was allowed to proceed for 30 min while the vessel remained on the 3-D rotator. Finally, the reaction solution was centrifuged for 15 min, the supernatant removed, and fresh, sterile PBS was added to the RBC pellet to bring the final Hb (within the RBC) concentration to approximately 1 mM. The modified RBCs were then stored at 4°C until analysis.

The capillary wetting system used in this study mainly consisted of a glass capillary tube of known radius (Polymicro Technologies, Phoenix, AZ). The capillary radius, R, ranged from 10.5 to 50 μm and the length is uniform around 15 cm. To further ensure that the suspension wets the capillary under the same condition and that the blood cells do not adhere to the capillaries, zeta potentials of the normal and cross-linked RBC suspensions were measured using a Zetapals instrument (Brookhaven Instrument Corp., Holtsville, NY). Each sample was prepared by adding one drop of the RBC suspension to 15 mL of either PBS or ILCM (isotonic low conductivity media, 10 mL of ILCM containing 8.6% w/w sucrose, 0.3% w/w dextrose, and 1.0 mg/mL BSA (Sigma), pH 7.4) medium. The instrument's noble metal electrode was preconditioned using either PBS or ILCM respectively (10 runs, 30 cycles). The medium used for preconditioning was then removed from the holding cell, and an aliquot of the RBC suspension was added to the holding cell and analyzed (10 runs, 20 cycles).

A large drop (volume ~40 μL) was placed in front of the capillary during each penetration experiment. The linear dimension of the drop was roughly 5 mm while the outer capillary diameter did not exceed 300 microns. The entire volume of blood that invaded into the capillary was estimated to not exceed 5 μL for the duration of the experiments, which was only a small fraction of the drop volume. A continuous supply of homogeneous blood suspension was hence provided by the drop.

The meniscus motion and the particle concentration were monitored using a high speed video camera (1,000 frames/s) attached to an inverted microscope as depicted in Figure 1. The field of view contained roughly a 200 μm section of the capillary, and video movies were recorded for 6 to 10 separate stations of known distance from the capillary entrance. Separate experiments were carried out for measurement and imaging at each station for a given R, ϕ_0, and drop volume placed at the capillary entrance.

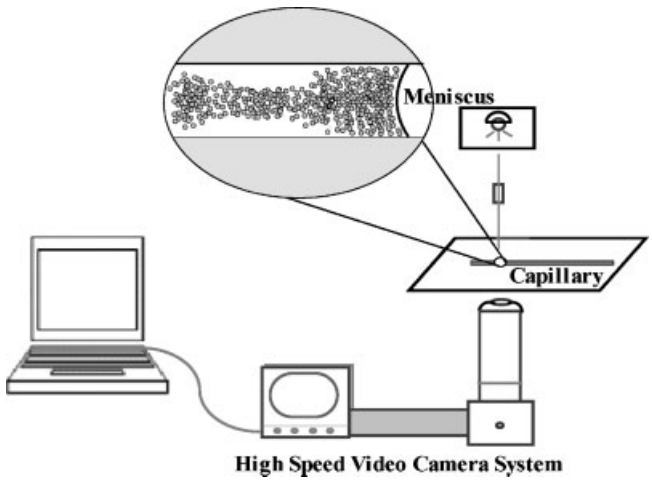

Figure 1. Schematic of experimental setup.

RESULTS AND INTERPRETATION

Assuming fully developed laminar flow in small capillaries, the supply of homogeneous RBC suspension to the moving meniscus can be modeled by a linear hydrodynamic resistance, which increases proportional to the length of the liquid plug. The driving force for the homogeneous liquid is the constant capillary pressure σ/R (Kalliadasis and Chang, 1996). This capillary pressure produces a pressure gradient of $\Pi = \sigma/RL$ across the wetted length of L. Using this gradient in the equation of motion in a cylinder yields a radially average liquid velocity $\langle u \rangle(t)$ as a function of the position of the moving meniscus $L(t)$:

$$\langle u \rangle(t) = R\sigma\cos(q)/8\mu L(t) \qquad (1)$$

where θ is the contact angle of the liquid to the capillary wall, σ the surface tension of the liquid in air, and μ the viscosity of the liquid. As the meniscus velocity profile is radially uniform, a simple flow balance then stipulates that $\langle u \rangle(t)$ is also the meniscus velocity at $L(t)$.

The viscosity dependence on concentration $\mu(\phi)$, ϕ being particle volume concentration, is typically different for RBCs and rigid particles. Typically, the following power-law constitutive equation for the viscosity is used to describe this dependence (Phillips et al., 1992):

$$\mu(\phi) = \mu_{\text{fluid}}(1 - (\phi/\phi_{\text{m}}))^{-v} \qquad (2)$$

Suspensions of rigid particles reach infinite viscosity at the maximum simple cubic packing volume fraction of $\phi_{\text{m}} = 0.62$, while deformable RBCs can be packed very densely such that their viscosity remains finite even at the maximum volume fraction of $\phi = 1$. As such, the nominal maximum volume fraction ϕ_{m} is found to be 1.1 from fitting the rheological data of Haynes and Burton (1959) such that the viscosity is finite for the entire physical range of ϕ. The singular power-law constitutive Equation (2) results in this non-physical ϕ_{m} because the true viscosity is finite. The plasma viscosity μ_{fluid} in Equation (2) is taken to be 1.0 cp and the exponent $v = 1.82$ was also obtained by fitting the blood viscosity data at $R = 747.7\mu$m of Haynes and Burton (1959). At a maximum packing of $\phi = 1.0$, the effective viscosity is about 100 times higher than that of pure plasma, an important fact that will be utilized in our theory for explaining penetration failure.

The above wetting theory assumes an RBC suspension with a homogeneous RBC distribution. However, considerable RBC segregation and aggregation were observed in our experiments. Images from high-speed video of normal RBC suspensions penetrating into capillaries showed a concentrated cell slug behind the meniscus (Fig. 2a), while latex particle suspensions remained homogeneous (Fig. 2b). Normal deformable RBCs behind the slug favored the capillary centreline (see top left of Fig. 2a), and a clear marginal layer free of cells appeared near the capillary wall. In dilute solutions, individual cells are observed to radially segregate and pack behind the meniscus immediately after it enters the capillary. Endotoxin-treated RBCs (Fig. 2c) also did not pack onto the meniscus as normal RBCs did, instead they behaved as latex particles and exhibited a more even distribution across the capillary. This observation indicates the reduced deformability of RBCs after treatment with an endotoxin can affect the RBC segregation in the penetrating flow.

A detailed RBC count at the steady state after the meniscus region in the radial direction produces the particle fraction distributions shown in Figure 2e for both normal and endotoxin-treated suspensions of Figure 2e. The count is carried out on video frames and hence reflects the true particle fraction distribution and not the flow-weighted distribution. It is clear that the distribution is much more

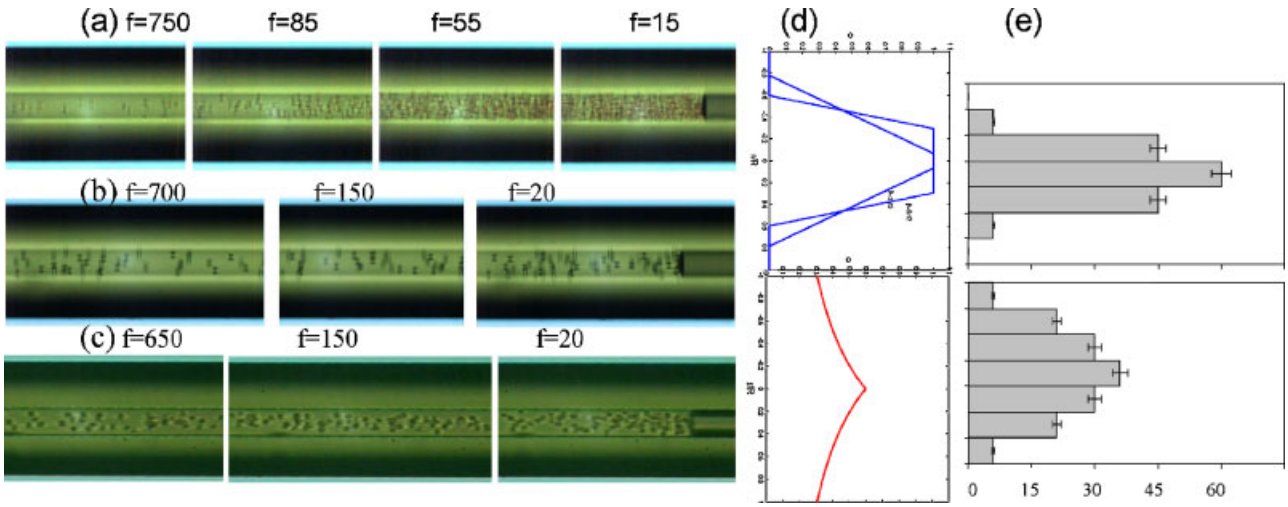

Figure 2. **a**–**c**: Images of advancing normal RBC (top), latex microspheres (middle), and endotoxin treated RBC (bottom) suspensions (both $\phi_0 = 1\%$) at $L = 2$ cm from the entrance for the indicated frame numbers. The frames are taken at 1,000 frame per second. In normal blood suspension (top), a concentrated unsegregated slug is formed behind the meniscus but blood cells remain radially segregated behind the slug. For latex and endotoxin treated RBC suspensions (bottom two), neither meniscus packing nor upstream radial segregation is observed. **d**: Computed radial blood cell distribution for rigid spheres (lower figure) and deformable spheres at $\beta = 3.85$ and 9.13. **e**: RBC counts for normal and endotoxin treated suspensions at frame ~700, which is far upstream of the meniscus, are compared to theoretical curves at two different values of the capillary number β. [Color figure can be seen in the online version of this article, available at www.interscience.wiley.com.]

homogeneous for the endotoxin-treated suspension. Although we are unable to determine whether the normal blood cells are deformed with the small images of the cells, we will deduce and confirm from theoretical analysis of the hydrodynamic data that the difference in the two distributions is due to particle deformability and the same difference accounts for the penetration failure of normal RBC suspensions into small capillaries.

The radial migration of normal RBCs towards the capillary axis creates a marginal layer near the capillary wall that has a small volume fraction of blood cells. This segregation phenomenon reduces the local hydrodynamic resistance, but also endows the segregated blood cells with a higher velocity. This average velocity is higher than the average liquid velocity, which is constant throughout the wetted region by flow balance and is hence equal to the meniscus velocity. As a result, the faster RBCs outrace the meniscus and pack behind it to form a slug with increasing concentration. The resistance at the slug finally dominates and arrests further meniscus advance. Careful scrutiny of the meniscus for different RBC concentrations shows minute contact angle changes due to absorption of the RBCs onto the contact line. However, the contact angle change does not seem to contribute significantly to the hydrodynamic resistance. Ironically, the radial migration which initially reduces hydrodynamic resistance by removing RBCs from the marginal layer, eventually causes a high-resistance slug to form behind the meniscus and induces loading failure.

The results from the three different levels of glutaraldehyde treated RBC suspensions confirm that glutaraldehyde cross-linking also reduced the deformability of RBCs, as shown in Figure 3. For suspensions treated with the highest glutaraldehyde concentration (Fig. 3c), RBCs became rigid and only slightly favored the capillary centreline. Their suspensions also did not exhibit appreciable packing at the meniscus. RBC suspensions treated with a medium glutaraldehyde concentration (Fig. 3b) showed more radial migration and meniscus packing and hence exhibited wetting dynamics somewhere between rigid and normal RBCs (Fig. 3a).

Penetration experiments were carried out with raw capillaries and prewetted ones, the latter were washed by PBS or a Fetal Bovine Serum solution (diluted 1:100 in PBS) for 15 min, followed by a 30 min water wash. The residual liquid inside was removed by connecting one end of the glass capillary with a vacuum, and checked under microscope prior to use. Penetration failure observed within 2 cm of the entrance was found to be independent of raw capillaries and prewetted ones. The concentration gradient from the packed meniscus to downstream was prominent and meniscus velocity differences were within measurement errors.

We did not observe RBC adhesion to the capillary in our experiments. One possible cause of adhesion is electrostatic attraction between the capillary wall and RBC. However, we found the RBC zeta potential to be the same sign as the capillary wall and also to be independent of cross-linking. Conversely, repulsive interactions between the like charges of RBCs and the capillary wall can also contribute to the observed radial segregation. However, by showing the RBC zeta potential to be independent of cross-linking, we also rule out this effect. The zeta potential of normal and cross-linked RBCs was measured with the RBCs suspended in either PBS or ILCM. When suspended in PBS, the instrument showed that the change in zeta potential of the RBCs was within the margin of error for the instrument (-13.507 ± 2.704 mV for normal RBCs and -13.87 ± 1.825 mV for RBCs cross-linked at a 2:1 molar ratio). The zeta potential of normal RBCs suspended in a low-conducting medium, ILCM, was found to be -35.70 ± 0.30 mV. However, the zeta potential again did not change significantly with cross-linking as the 2:1 molar ratio cross-linked RBCs were found to have a potential of -34.65 ± 0.36 mV. Data were obtained from at least two measurements for each suspension. Therefore, the electrical interaction between the RBCs and the glass wall of the capillary is not expected to change significantly with

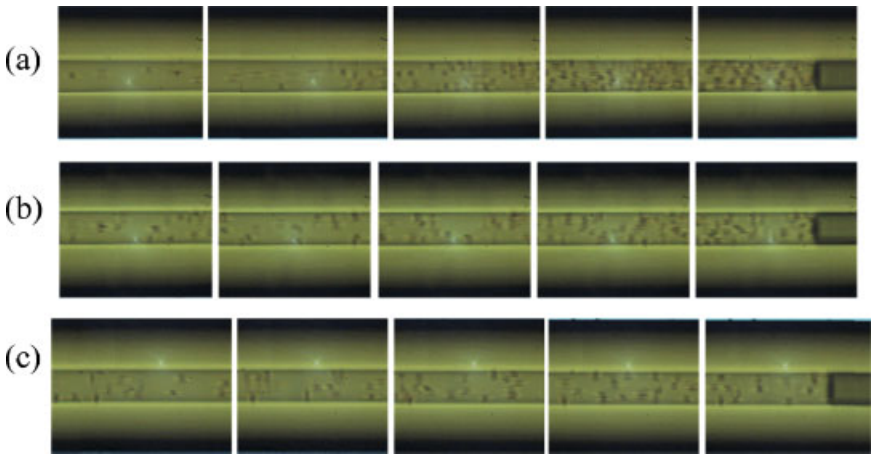

Figure 3. Images of advancing meniscus using suspensions with blood cells cross-linked with different concentrations of glutaradehyde. Image (**a**) corresponds to normal RBCs without cross-linking. Image (**c**) corresponds to the highest glutaraldehyde concentration (2:1), when neither concentrated slug nor upstream segregation is formed behind the meniscus. Image (**b**) is a transitional stage between rigid and deformable blood cells with a glutaraldehyde concentration ratio of 1:1. [Color figure can be seen in the online version of this article, available at www.interscience.wiley.com.]

cross-linking, and thus its impact on capillary wetting and meniscus packing should not change significantly. Hence, the observed segregation and packing phenomena, which are sensitive to cross-linking, are not due to electrostatic interaction between the RBC and the capillary wall. RBC sedimentation is not observed during all the wetting experiments. We estimate the sedimentation time for blood cells in the 100 micron capillary to be 5 min while our wetting experiment is over in less than 30 s.

While the concentrated RBC slugs were observed for all conditions of normal deformable RBCs, the wetting dynamics depart from the homogeneous wetting speed produced by Equation (1) only for high initial RBC volume fraction ϕ_0 and small capillary radius R. In Figure 4, the relationship between entrance length and recorded meniscus velocity $\langle u \rangle$, after normalization by the homogeneous suspension velocity (1), is shown to approach the theoretical prediction only at small ϕ_0 and large R. The slight scatter of about 10 % from (1) is mostly due to the inaccuracy of our viscosity constitutive equation (2) used to estimate the wetting velocity of a homogeneous suspension. For high ϕ_0 and small R, $\langle u \rangle$ is found to drop precipitously over a short distance of less than 1 cm from the entrance and to deviate from homogeneous wetting. The meniscus essentially stops completely within this length. The measured critical concentrations ϕ_c, beyond which this penetration failure occurs, are shown in Figure 5a for different capillary radii R. The meniscus of every failed penetration experiment contained a slug of highly packed RBCs. The concentrated slugs behind the meniscus were observed even if the penetration was successful, in which case their particle concentration grew downstream but never approached those of failed penetrations. The slug began to develop when the meniscus was at the entrance. Although the particle concentration within the slug increased down stream, the slug length L_{slug} for normal RBCs was not found to vary significantly downstream. However, the slug length's measured value was seen to be a strong increasing function of the capillary radius (Fig. 5b).

For endotoxin treated RBC suspensions, the meniscus velocity was found to be close to that predicted by the homogeneous theory. A concentrated slug never formed behind the meniscus and penetration failure was never observed. In Figure 6, wetting velocities for normal RBCs and endotoxin treated RBC suspensions at the critical concentration ϕ_c of normal RBCs were compared for a 21 μm capillary. Instead of a precipitous drop in meniscus

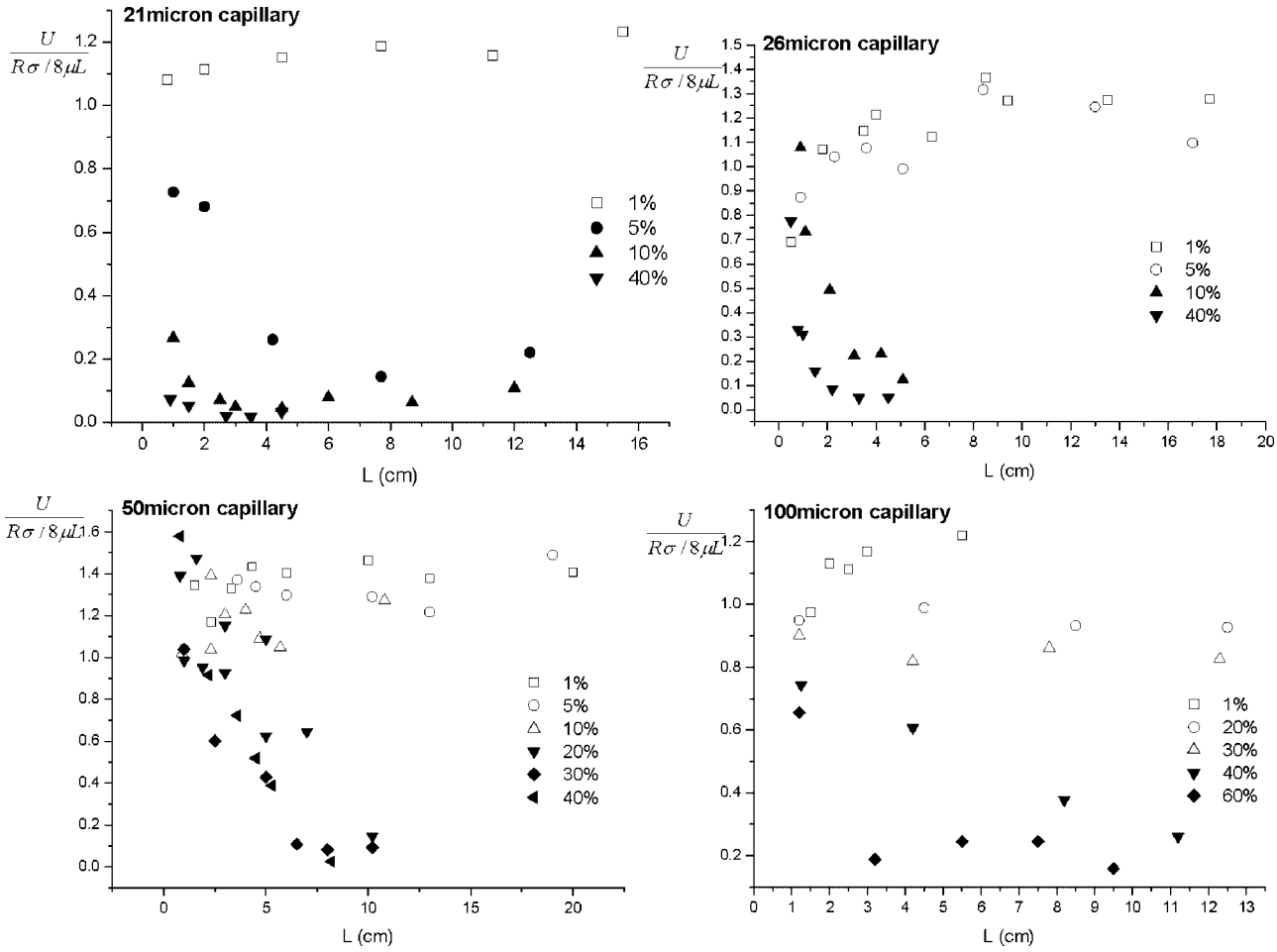

Figure 4. Scaled meniscus velocities versus the wetted length L. The precipitous drop in the velocity for concentrations beyond the critical concentration is evident for each of the four capillaries used.

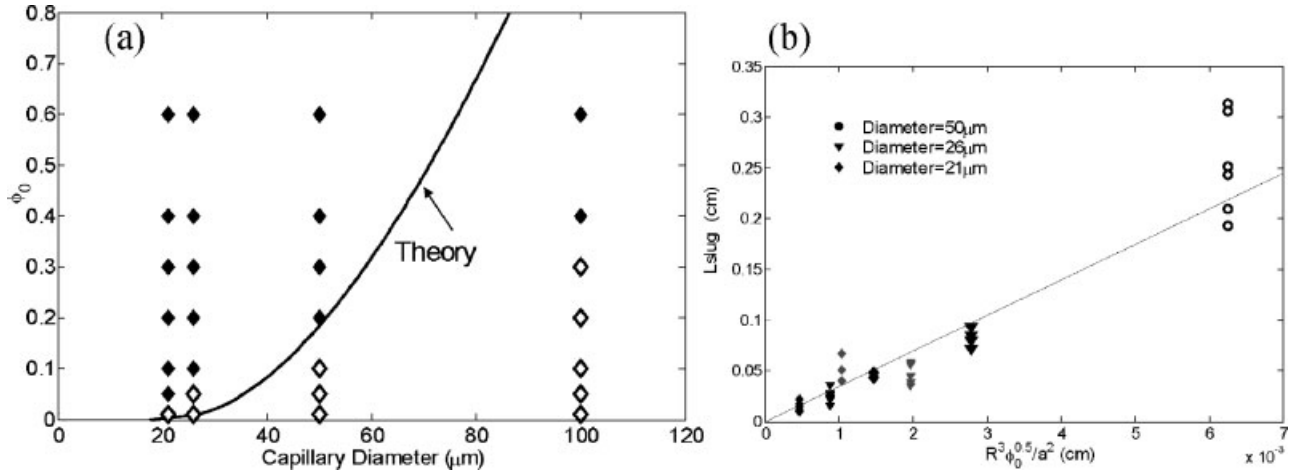

Figure 5. **a**: Critical penetration condition in the concentration - diameter parameter space. The open diamonds correspond to homogeneous wetting and the closed diamonds arrested wetting due to the packing mechanism. The curve is our theoretical result. **b**: Measured slug length for three capillary diameters $D = 2R$ and three concentrations (open symbol 10%; blue symbol 5%; closed symbol 1%) compared to our theoretical scaling from balancing rigid particle radial migration with longitudinal convection.

velocity, endotoxin treated RBC suspensions exhibited a wetting velocity consistent with that of a homogeneous suspension in (1). We shall show that this tendency towards homogeneous suspension is endowed by the rigidity of the endotoxin-treated RBCs. This would be consistent with earlier speculations that endotoxin treated RBCs are more rigid (Baskurt et al., 1998; Hinshaw, 1996).

Experiments at the capillary entrance also showed that a marginal layer clear of particles existed near the wall for all blood cells (Fig. 7). Averaging the particle separation from the wall for the experiment in Figure 7 over hundreds of imaging frames, each corresponding to a 1 cm wetting length, yields an average marginal layer of 10 microns at the entrance. The existence of such an entrance layer is apparently independent of the rigidity of the RBC. Its thickness is roughly the particle radius a, suggesting that the marginal layer is produced by an excluded volume effect at the entrance such that the particle cannot be less than one particle radius away from the wall. While such a marginal layer due to excluded volume effects is always present, it reduces the induction length L_t for radial migration at small capillary radii R. This is evident in Figure 7c where a thick marginal layer developed when the entrance marginal layer was further thickened by subsequent radial migration of RBCs from the wall at a low advancing velocity.

THEORY AND DISCUSSION

The above results suggest different mechanisms are at play for the anomalous wetting dynamics of both deformable RBCs and rigid RBCs in small capillaries. The wetting process can be divided into three regions, the entrance transition region, the intermediate migration region and the

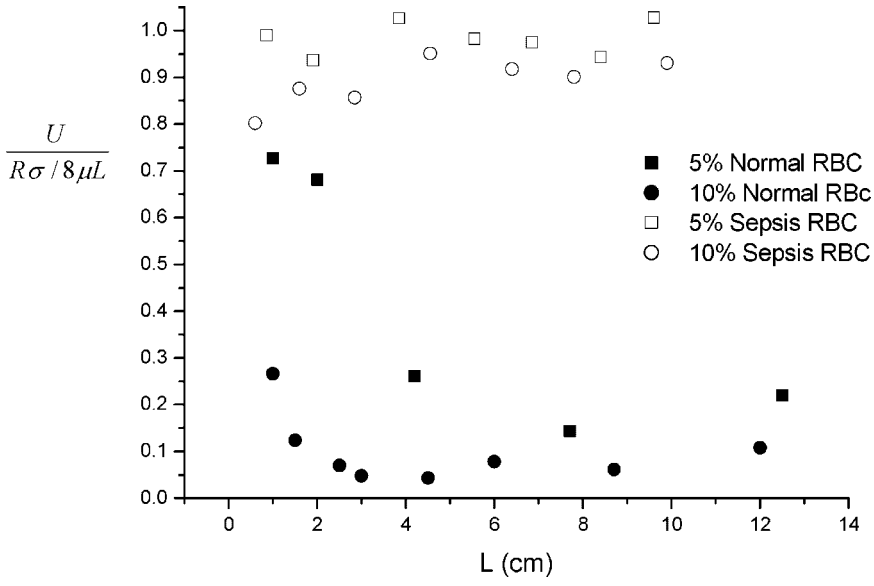

Figure 6. Normalized velocity evolution for normal RBC suspensions and endotoxin treated RBC suspensions in a 21 micron capillary.

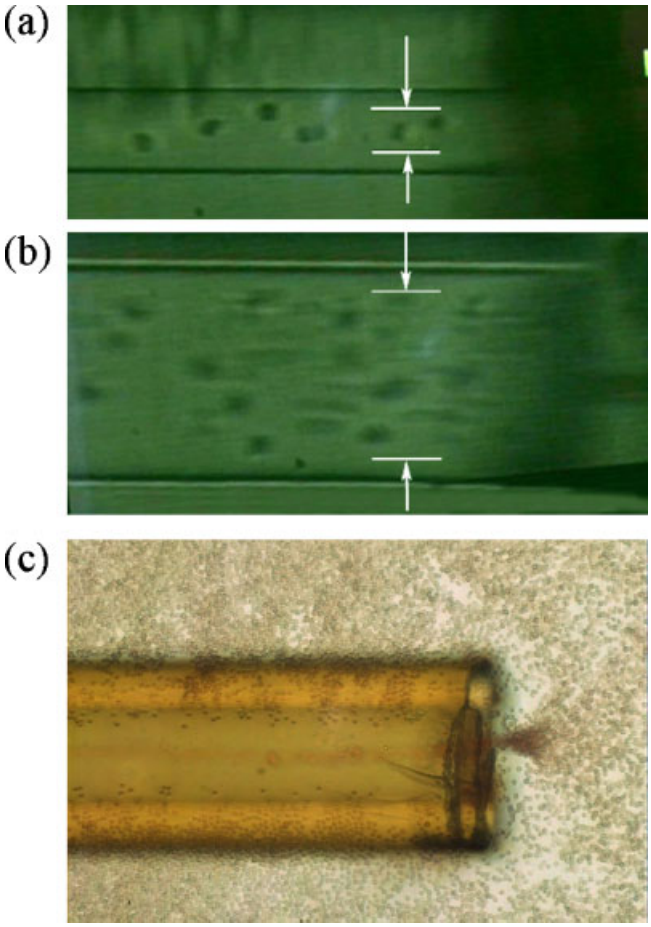

Figure 7. Excluded volume effect for (**a**) $R = 10.5$ μm, $\phi_0 = 1\%$ (**b**) $R = 25$ μm, $\phi_0 = 1\%$. The cone formation in image (**c**) suggests that shear induced migration occurs at the entrance of capillaries (c). The plasma layer is roughly 10 microns for (a) and (b). The corners are cut with a ceramic cutter and its sharpness is difficult to control. However, the corner geometry does not seem to affect the cone formation phenomenon. [Color figure can be seen in the online version of this article, available at www.interscience.wiley.com.]

slug pack region. Deformable RBCs favored the centreline during the intermediate region and moved with a higher average particle velocity $\langle u_p \rangle$ than a homogeneous suspension with average fluid velocity $\langle u \rangle$. At the liquid front, the meniscus must move at the average fluid velocity $\langle u \rangle$ due to flow balance. Consequently, the RBCs outraced the liquid plasma and packed behind the meniscus to form the concentrated and radially unsegregated slug. The slug concentration, ϕ_{slug}, increases in time at a rate proportional to the flux from the segregated region, and hence increases with ϕ_0. As the RBC suspension viscosity in Equation (2) has been shown to be as much as 100 times larger than pure plasma at a maximum volume fraction of $\phi = 1.0$, viscous resistance at the slug eventually arrests further blood penetration into the capillary, and velocity is thus significantly decreased. However, for rigid RBCs, particles are not segregated and the average particle velocity is the same as the meniscus velocity. This results in no RBC packing onto the meniscus and similar wetting dynamics to that of homogeneous liquid. However, the migration and diffusion mechanisms at the different regions can be very different, and consequently a more careful modeling attempt will be developed in the subsequent sections to quantitatively estimate the critical penetration condition in Figure 5a for normal blood suspension with deformable RBCs.

Radial Segregation Model for Intermedial Region

Within the intermediate region, we adopted a radial migration model for deformable drops that was previously suggested by King and Leighton (2001), which combines the deformation term derived by Chan and Leal (1979) with a term that combines shear-induced migration and self-diffusion (Leighton and Acrivos, 1987; Phillips et al., 1992) to produce the radial particle flux for a radially distributed RBC volume fraction ϕ (r),

$$N_r = -k_d(\gamma a\ \mu/\sigma_{cell})\ \gamma a\ (ar)/(R^2)\phi - D(\partial\phi/\partial r) \quad (3)$$

where the local suspension viscosity $\mu(\phi)$ is taken to be the bulk value of Equation (2), k_d is a universal constant, a is the particle (RBC) radius, σ_{cell} is the effective membrane tension, and γ is the local shear rate which has a characteristic value of $\langle u \rangle / R$ for a capillary. The first term within Equation (3) is due to shear-induced migration of a deformable particle with a migration velocity of k_d $(\gamma a \cdot \mu/\sigma_{cell})$ γa $(ar)/R^2$ due to particle deformation. The second term, with a diffusion coefficient $D = \lambda \cdot \gamma a^2 \phi$, describes diffusion down concentration gradients due to particle-particle interaction (λ is a constant including contributions from both self-diffusivity and gradient-induced drift). We have omitted viscosity gradient driven diffusion (Phillips et al., 1992), which is estimated to be unimportant for realistic concentrations, to produce a single dimensionless parameter.

The scaling with respect to γ is different for the two terms within the flux equation and the ratio between the two, a sort of Peclet number balancing migration velocity and diffusion homogenization, yields a unique dimensionless parameter that determines the relative strength of radial migration due to the deformability of blood cells to that of diffusion due to multi-particle interaction of rigid particles,

$$\beta = (2k_d/9\lambda\sigma_{cell})(a\Pi R/\phi_0) \quad (4)$$

This parameter is also analogous to the capillary number, which measures the ratio of the viscous shear force to surface tension. This parameter specifies the degree of segregation of the RBCs. We took King and Leighton's empirical value of $\lambda = 0.3$, k_d was fitted to be 0.012 subsequently, and σ_{cell}, was taken to be 4×10^{-4} mN/m for a RBC from the AFM force measurements of Tachev et al. (18). The pressure gradient Π, is related to the characteristic shear rate γ, through a force balance, $\Pi \sim \gamma\mu/R$. This term is the pressure gradient of a particular flow channel, and can also be deduced from the flow rate if a homogeneous fluid is assumed.

In contrast, the shear-induced migration rate for a rigid particle has a migration velocity quite distinct from the deformation induced mechanism. In this case, we balance the

migration by not just the concentration gradient diffusion term in Equation (3) but also the viscosity gradient term, as was done by Phillips et al. (1992),

$$N_r = -k_c a^2(\phi^2 \partial\gamma/\partial r + \phi\gamma\partial\phi/\partial r + \delta\phi^2\gamma(d\ln\mu/d\phi)\partial\phi/\partial r) \quad (5)$$

The third term, which accounts for a viscosity gradient ($\delta = 1.52$), is typically small for practical concentrations, but is retained here for completeness. Its existence does not produce an additional dimensionless parameter here as all three terms have the same scaling in Equation 5. As a result of this identical scaling, steady radial ϕ distribution in well-developed capillary flow, defined by $N_r = 0$, is a universal one independent of all parameters. This universal rigid particle concentration profile can be obtained explicitly for the power-law viscosity constitutive Equation (2) as a function of a dimensionless radius scaled by the capillary radius R. It is shown in Figure 2b and the distribution only slightly favors the centreline. The ''induction'' period for this equilibrium is $R^2/\gamma a^2\phi$ and the induction length is $L_t = (R^3/a^2\phi)$, as was derived earlier.

For deformable particles, the equilibrium distribution must be determined numerically by simultaneous solution of the radial flux Equation (3) with the equation of motion driven by a constant pressure gradient Π

$$\frac{1}{r}\frac{\partial}{\partial r}\left(\mu(\phi)\frac{\partial u}{\partial r}\right) = \Pi \quad (6)$$

As the scaling of the deformation mechanism in Equation (3) is different from the diffusion mechanism, a universal distribution is impossible. Instead, the normalized distribution (ϕ^*/ϕ_0) is a function of (r/R) and the unique parameter β in Equation (4). We have obtained these profiles as functions of β (shown in Fig. 2d for two different β values) by solving the flux Equation (3) and the equation of motion Equation 6 simultaneously with particle and fluid flux balances. The clear plasma layer develops at $\beta_c = 15/7$. At large β values with high shear, a focused particle distribution develops on the capillary centreline. Due to RBC deformation, this shear-induced migration is much stronger for deformable cells than for rigid ones at a high shear rate for capillary wetting experiments. This explains the lack of segregation seen in both latex particle and endotoxin treated RBC suspensions (Fig. 1) during capillary wetting experiments.

From the above arguments, it is clear that, unlike rigid particles, the apparent viscosity of a suspension of deformable RBCs is a function of the single dimensionless parameter β. In Haynes and Burton's data for continuous capillary flow without a meniscus, the apparent viscosity is observed to increase with R for constant flow rate, Q, experiments, but to decrease with R for constant pressure-drop experiments, which is in contradiction to the rigid particle model. Haynes and Burton's effective viscosity estimate contains some error for capillary diameters below 300 microns, and consequently Merrill et al. (1965) corrected for the hematocrit difference between the homogeneous suspensions and segregated ones. Nevertheless, the pertinent scaling we shall scrutinize is why the apparent viscosity scales differently with respect to R for constant flow rate and constant pressure-drop experiments, and we shall examine their data with R spanning more than one order of magnitude. This apparent contradiction is explained by the β scaling of $\Pi R/\phi_0$ which introduces a new R scaling through Q. As Q scales as ΠR^2, a constant Q experiment would correspond to a β that scales as $1/R$ instead of the R scaling for a constant pressure drop experiment with Π constant. In Figure 8, we collapse all given Π and Q data for apparent viscosity μ, scaled by the plasma viscosity μ_0 of Haynes and Burton

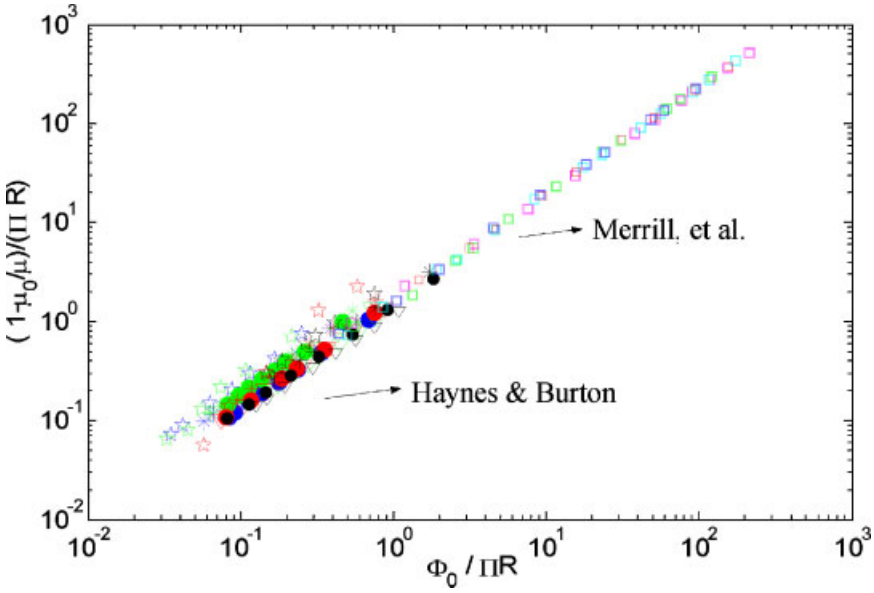

Figure 8. Collapsed data of Haynes and Burton (1959) and Merrill et al. (1965) (in square symbols) for whole blood flow in capillaries of radius R at fixed pressure and flow rate. The horizontal axis of ($\phi_0/\Pi R$) has the same scaling as β. The data of Merrill et al. are for $\phi_0 = 39.3\%$ and $R = 144$ μm, 183 μm, 192 μm, 261.5 μm, and 425 μm. [Color figure can be seen in the online version of this article, available at www.interscience.wiley.com.]

(1959), and Merrill et al. (1965) into a universal curve that depends only on $\phi_0/\Pi R$, the β scaling. If deformability is not a factor, the apparent viscosity would not be a function of β and thus should not collapse into a single universal curve in Figure 8. The collapsed data spans $0 < \phi_0 < 0.83$, 50 μm $< R <$ 750 μm and $0 < \Pi < 160$ mmH_2O/cm. This excellent collapse underscores the importance of deformation in blood rheology and the accuracy of our constitutive equations. The error in the volume fraction ϕ_0, may contribute to the scatter, but perhaps due to the small range of volume fraction used, it did not significantly corrupt the collapse.

We note that the value of β decreases with increasing particle concentration ϕ. At the small β limits, deformable particles behave like rigid ones and (5) should be used. This explains the scatter at small β and the better collapse at larger β. Hence, the deformability of the RBCs is unimportant in the packed region behind the meniscus. We shall hence use the rigid particle scalings to estimate the maximum penetration length of the meniscus by carrying out a particle balance in the packed region.

Packed Region

While radial migration and segregation of erythrocytes produces a lower apparent viscosity in well developed and continuous capillary blood flow driven by a pump, they can have an opposite effect in wetting flow with an advancing meniscus. The radially segregated erythrocytes pack behind the meniscus as they possess a larger average speed than the meniscus speed. If the packing occurs near the entrance, the packed slug with elevated hydrodynamic resistance occupies a significant portion of the wetted length, and capillary penetration is arrested. If the packing occurs far from the entrance, however, the lubricating and viscosity reducing effect of the dominant segregated region prevails.

At the meniscus, radial migration disappears as the radial shear gradient vanishes for the flat plug-flow velocity profile at the meniscus. Instead, the diffusion process due to the radial concentration gradient drives the blood cells to the wall with a diffusivity that also scales as $\phi_0\langle\gamma\rangle a^2$, where $\phi_0\langle\gamma\rangle$ captures the collision frequency that drives this diffusion process (Leighton and Acrivos, 1987). The slug length, L_{slug}, can hence be interpreted by a balance between the radial diffusion time $R^2/\phi_0 \cdot \gamma a^2$ and the longitudinal convection time $L_{slug}/\langle u\rangle \sim L_{slug}/(R \cdot \gamma)$, and is identical to the induction length L_t for segregation. Due to their identical scaling, the segregation length for shear-induced migration is identical to the ''homogenization'' length due to diffusion. This yields a L_{slug} whose R^3 scaling is in good agreement with our measured slug length in Figure 3b. There is a different ϕ_0 dependence through blood cell deformation, and consequently we improve the above scaling empirically to $L_{slug} \sim 35.0(R^3/a^2)(\phi_0)^{1/2}$ to produce the good collapse of measured data for a wide range of RBC concentrations and capillary radii in Figure 5b.

Once the volume fraction within the slug reaches maximum packing, the hydrodynamic resistance of this slug far exceeds that in the rest of the wetted region. This claim can be estimated by the fact that the viscosity at maximum packing is about 100 times that of the plasma from Equation (2). This implies that the effective resistance of the well-packed slug is roughly equivalent to that of plasma over a length of 100 L_{slug}. With the estimate of Figure 5b, this corresponds to about 3.5×10^3 (R^3/a^2) or 5 m for a capillary of radius $R = 50$ microns and for whole blood. This value far exceeds (by two orders of magnitude) the resistance in the rest of the wetted region in the 15 cm capillaries. We can hence safely assume that the wetting penetration fails when the packing reaches the maximum value of $\phi = 1$ in the slug. This estimate allows us to determine from a particle balance in the slug the meniscus position (the maximum penetration depth) when the meniscus advance is arrested.

Since L_{slug} is constant throughout the capillary penetration, the blood accumulation rate in the slug is described by

$$d\phi_{slug}/dt = (\langle u\phi\rangle - \langle u\rangle\langle\phi\rangle)/L_{slug} \tag{7}$$

where $\langle\cdot\rangle$ denotes the cross-sectional average. A totally segregated suspension with all particles along the centreline would yield an initial packing rate of $\langle u\phi\rangle - \langle u\rangle\langle\phi\rangle \sim \langle u\rangle\phi_0$ as the centreline velocity, which is twice the average velocity $\langle u\rangle$ in Poiseuille flow. With this approximation, Equation (4) yields a correlation between the slug concentration ϕ_{slug} and the meniscus position (wetted length) L, $(\phi_{slug}/\phi_0) \sim (L/L_{slug})$. The wetted length for the slug to reach maximum packing or the maximum penetration depth, L_{max}, can hence be estimated by setting ϕ_{slug} to unity,

$$L_{max} = L_{slug}/\phi_0 = 35.0(R^3/a^2)/\phi_0^{1/2} \tag{8}$$

Entrance Region

There is an entrance region within the capillary where the RBCs segregated radially. The length of this entrance region is nominally the induction length L_t for shear-induced migration. However, the entrance marginal layer due to excluded volume effects can significantly reduce this length for small capillaries. Consider a marginal layer thickness of b, the particles need only migrate the reduced distance $(R-b)$ and the entrance transition length, L_t, is then corrected to

$$L_t \sim \langle\gamma\rangle R(R-b)^2/\langle\gamma\rangle\phi a^2 \tag{9}$$

The segregated region is hence sandwiched between the entrance transition region and the concentrated meniscus slug. Precipitous drops occur when the segregated region is vanishing short and the maximum packing, L_{max}, is reached as soon as the RBCs leave the entrance transition region

$$L_{max} = L_t + L_{slug} \tag{10}$$

An estimate of the critical capillary radius R_c, for penetration failure of normal blood with deformable RBCs can thus be obtained as a function of ϕ_0 by relating (8), (9)

and (10),

$$(R_c/a) = 1.77(1 + 1.04\phi_0^{1/4} + 1.38\phi_0^{1/2} + 1.97\phi_0^{3/4}) \quad (11)$$

This theoretical prediction is in good agreement with the data in Figure 5a. For whole blood at $\phi_0 = 40\%$, the theory predicts that the penetration failure occurs when the capillary radius R is below 40 microns. This is consistent with the rule of thumb in the diagnostic industry.

This validates our theory that shows the existence of an entrance marginal layer due to excluded volume effects, an intermediate radial segregation region due to deformation or shear-induced migrations depending on the rigidity of the RBCs and a shear-induced concentration gradient-driven diffusion region at the packed slug right behind the meniscus. A large number of the reported particle segregation mechanisms are hence present. However, the rigid particles segregate only weakly, as seen in their universal equilibrium particle distribution in Figure 2b, compared to the severely segregated distribution of deformable particles in Figure 2a at large β. As a result, significant meniscus packing and penetration failure only occur for deformable RBCs.

CONCLUSION

We have shown that capillary loading of blood suspensions by wetting is sensitively affected by the deformability of the erythrocyte. The deformed red blood cells migrate away from the wall and pack behind the meniscus to form a concentrated slug, whose large hydrodynamic resistance eventually arrests the advance of the wetting meniscus. This radial migration is enhanced by an entrance excluded volume effect when the capillary radius approaches the particle dimension. These mechanisms combine to produce a critical capillary radius for loading that is concentration and deformability dependent. We have demonstrated that endotoxin treated RBCs and glutaraldehyde fixed RBCs are indeed rigid. The fact that these blood suspensions do not lead to loading failure suggests some possible designs (Srivastava et al., 2005) of sepsis diagnostic kits, which will be reported in a subsequent paper.

This work is supported by a NASA grant NAG5-10503. We are grateful to Dmitri Lastochkin for assistance in collecting the data of Figure 3 David T, Leighton and Ping Wang for valuable discussions and assistance.

References

Baskurt OK, Gelmont D, Meiselman HJ. 1998. Red blood cell deformability in sepsis. Am J Resp Crit Care Med 157(2):421–427.

Bellelli A, Benedetti PL, Coletta M, Ippoliti R, Brunori M. 1988. Human-erythrocytes cross-linked with glutaraldehyde general-properties and significance as a blood substitute. Biochem Biophys Res Commun 156(2):970–977.

Brooks DE, Goodwin JW, Seaman GVF. 1970. Interactions among erythrocytes under shear. J Appl Physiol 28(2):172–177.

Chan PC-H, Leal LG. 1979. The motion of a deformable drop in a second-order fluid. J Fluid Mech 92:131–170.

Fahraeus R, Lindqvist T. 1931. The viscosity of the blood in narrow capillary tubes. Am J Physiol 96:562–568.

Goldsmith HL, Mason SG. 1962. The flow of supsension through tubes. I. Single spheres, rods, and discs. J Coll Sci 17(5):448–476.

Haynes RH, Burton AC. 1959. Role of the non-Newtonian behaviour of blood in hemodynamics. Am J Physiol 197:943–950.

Hinshaw LB. 1996. Sepsis/septic shock: Participation of the microcirculation: An abbreviated review. Crit Care Med 24(6):1072–1078.

Kalliadasis S, Chang H-C. 1996. Effects of wettability on spreading dynamics. Ind Eng Chem Res 35(9):2860–2874.

King MR, Leighton DT. 2001. Measurement of shear-induced dispersion in a dilute emulsion. Phys Fluids 13(2):397–406.

Leighton D, Acrivos A. 1987. The shear-induced migration of particles in concentrated suspensions. J Fluid Mech 181:415–439.

Merrill EW, Benis AM, Gilliland ER, Sherwood TK, Salzman EW. 1965. Pressure–flow relations of human blood in hollow fibers at low flow rates. J Appl Physiol 20(5):954–967.

Minerick AR, Ostafin AE, Chang HC. 2002. Electrokinetic transport of red blood cells in microcapillaries. Electrophoresis 23(14):2165–2173.

Olla P. 1999. Simplified model for red cell dynamics in small blood vessels. Phys Rev Lett 82(2):453–456.

Oser BL. 1965. Hawk's physiological chemistry. New York: McGraw Hill Book Company.

Phillips RJ, Armstrong RC, Brown RA, Graham AL, Abbott JR. 1992. A constitutive equation for concentrated suspensions that accounts for shear-induced particle migration. Phys Fluids a-Fluid Dynamics 4(1):30–40.

Pries AR, Neuhaus D, Gaehtgens P. 1992. Blood-viscosity in tube flow-dependence on diameter and hematocrit. Am J Physiol 263(6):H1770–H1778.

Saffman PG. 1965. The lift on a small spheere in a slow shear flow. J Fluid Mech 22:385–400.

Srivastava N, Davenport RD, Burns MA. 2005. Nanoliter viscometer for analyzing blood plasma and other liquid samples. Anal Chem 77(2): 383–392.

Tachev KD, Angarska JK, Danov KD, Kralchevsky PA. 2000. Erythrocyte attachment to substrates: Determination of membrane tension and adhesion energy. Coll Surf B-Biointerf 19(1):61–80.

Zhou R, Chang H-C. 2005. Capillary penetration failure of blood suspensions. J Coll Interf Sci 287(2):647–656.